Polym. Bull. (2012) 69:29–47
DOI 10.1007/s00289-011-0686-6

ORIGINAL PAPER

Synthesis, properties, and electrical memory characteristics of new diblock copolymers of polystyrene-*block*-poly(styrene-pyrene)

Pei-Hsuan Lin · Wen-Ya Lee · Wen-Chung Wu · Wen-Chang Chen

Received: 28 September 2011 / Revised: 30 October 2011 / Accepted: 3 December 2011 /
Published online: 11 December 2011

Abstract In this study, we report the synthesis, properties, and electrical memory characteristics of new diblock copolymers, polystyrene-*block*-poly(styrene-pyrene) (PS-*b*-P(St-Py)), prepared by combining atom transfer radical polymerization and Suzuki coupling reaction. The effects of the St–Py block chain length on the electronic energy level, photophysical properties, and memory characteristics were explored. The PS_{42}-*b*-$P(St\text{-}Py)_{108}$ and PS_{66}-*b*-$P(St\text{-}Py)_{67}$ devices exhibited a dynamic random access memory characteristics with different turn-on threshold voltages of −2.7 and −3.1 V, respectively. Moreover, these memory devices showed a high ON/OFF current ratio of 10^9 and were electrically stable for at least 10^4 s in both ON and OFF states. However, the PS_{113}-*b*-$P(St\text{-}Py)_{45}$-based device displayed an insulating state in a low current variation of 10^{-12} to 10^{-14} A, which had a short St–Py block length. The mechanism of the switching behavior was explained by the charge hopping conduction between the pyrene units with coexisting charge-trapping environment. The volatility of the memory effect was depended on the ability of charge trapping/back transferring of trapped charge.

Electronic supplementary material The online version of this article (doi: 10.1007/s00289-011-0686-6) contains supplementary material, which is available to authorized users.

P.-H. Lin · W.-C. Chen (✉)
Institute of Polymer Science and Engineering, National Taiwan University,
No. 1, Sec 4, Roosevelt Road, Taipei 10617, Taiwan
e-mail: chenwc@ntu.edu.tw

W.-Y. Lee · W.-C. Chen
Department of Chemical Engineering, National Taiwan University,
No. 1, Sec 4, Roosevelt Road, Taipei 10617, Taiwan

W.-C. Wu (✉)
Department of Chemical Engineering, National Cheng Kung University,
No. 1 University Road, Tainan 701, Taiwan
e-mail: wcwu@mail.ncku.edu.tw

The present study suggested that the electrical memory characteristics could be efficiently tuned through the block ratio between insulating segment and pendant-conjugated segment of the diblock polymers.

Keywords Diblock copolymer · Pyrene · Synthesis · Electrical memory · Charge transporting

Introduction

Polymeric and organic bistable memory devices are promising candidates for high-density data storage devices [1–7] because of their attractive features including simplicity in device structure, good scalability, low-cost potential, low-power operation, and three-dimensional stacking capability [8–11]. Electronic resistive-type memory devices using polymers as active elements are shown to efficiently store the data based on the high- and low-conductance response to an applied voltage. Several organic and polymeric memory materials composed of sandwiched layers exhibit memory switching characteristics, including small molecules [12–14], conjugated polymers [15–19], non-conjugated polymers (functional polyimide systems [20–24] or polymers with specific pendant chromophores [25–30]), and polymer nanocomposites (metal nanoparticle [11, 31–33] or fullerene [34–37] embedded). In contrast to wholly π-conjugated linear polymers, non-conjugated polymers containing pendant π-conjugated moieties [25–30] are of interest for their advantages of excellent solubility, tunable morphology, and precisely optoelectronic properties. However, the electrical switching memory behaviors of such polymers have not been fully explored.

We are particularly interested in the development of the polymers with pendant-conjugated moieties for resistive-type memory device applications [38–41]. For examples, polymers with pendant carbazole-containing groups exhibited hole-transporting ability that dominated the conduction. Conformation-induced electrical bistability in pendant polymer with carbazole units exhibited the WORM and SRAM switching effect [30, 38]. We have explored the electrical memory characteristics of non-conjugated random copolymers containing pendent electron-donating 9-(4-vinylphenyl)carbazole (VPK) or 4-vinyltriphenylamine (VTPA), and electron-accepting 2-phenyl-5-(4-vinylphenyl)-1,3,4-oxadiazole (OXD) or 2-(4-vinylbiphenyl)-5-(4-phenyl)-1,3,4-oxadiazole (BOXD). The electrical switching behavior of such random copolymers could be tuned through the donor/acceptor ratio or characteristics of pendant groups [39, 40]. Also, we discovered the well-correlation of the electrical memory characteristics with the pendant conjugated chain length in polystyrene derivatives with electron-donating oligofluorene pendant moieties [41]. The pyrene-containing polymers have been regarded as a fluorescent probe for monitoring conformational changes and molecular interactions, because their photophysical and photochemical properties are sensitive to environmental changes such as temperature, polarity, rigidity, and relative proximity [42–45]. However, the pyrene-containing polymers have not been explored for electrical memory device applications.

In this article, we report the synthesis, optoelectronic properties, and memory device applications of non-conjugated diblock copolymers containing pendant pyrene groups, polystyrene-*block*-poly(styrene-pyrene) (PS_n-*b*-$P(St\text{-}Py)_m$). Herein, PS_n-*b*-$P(St\text{-}Py)_m$ with three different block ratios (*n*/*m*) were synthesized by applying atom transfer radical polymerization (ATRP) first and subsequent with Suzuki coupling reaction. The effects of the pyrene content on the optoelectronic properties and memory characteristics of these copolymers were explored.

Experimental

Materials

N,*N*,*N*′,*N*″,*N*″-pentamethyldiethylenetriamine (PMDETA, 99+%, Acros), 1,1,4,7, 10,10-hexamethyl-triethylenetetramine (HMTETA, 97%, Aldrich), 1,4,8,11-tetramethyl-1,4,8,11-tetraazacyclotetradecane (Me_4cyclam, 98%, Aldrich), copper(I) bromide (CuBr, 98%, Aldrich), methyl 2-bromopropionate (98%, Aldrich), tetrakis(triphenylphosphine)-palladium(0) ($Pd(PPh_3)_4$, TCI), potassium phosphate tribasic (K_3PO_4, Aldrich), trioctylmethylammonium chloride (Aliquat® 336, Aldrich), pyrene-1-boronic acid (Lumtec), and *n*-butyllithium (*n*-BuLi, and 2.5 M in cyclohexane/hexane (92/8), Chemmetall) were used without further purification. Tetrahydrofuran (THF, anhydrous, TEDIA), anisole (Aldrich, 99.7%), and methanol were used as received. Styrene (99+%, Aldrich) and 4-bromostyrene (98%, Alfa Aesar) were passed through a base Al_2O_3 column prior to polymerization to remove the inhibitor.

General procedures for polymerization

The general procedure of synthesizing PS_n-*b*-$P(St\text{-}Py)_m$ is shown in Scheme 1. The polystyrene macroinitiator, the poly(4-bromostyrene) homopolymer, and the polystyrene-*block*-poly(4-bromostyrene) (PS-*b*-P4BrS) diblock copolymer were synthesized by ATRP. Then, Suzuki coupling reaction was applied with pyrene-1-boronic acid to afford the poly(styrene-pyrene) (P(St-Py)) homopolymer and the polystyrene-*block*-poly(styrene-pyrene) (PS-*b*-P(St-Py)) diblock copolymers.

Polystyrene macroinitiator (PS-Br)

CuBr (83.2 mg, 0.58 mol) was added to a dry three-neck flask with a magnetic stirring bar and sleeve stoppers. Styrene (10 mL, 86.4 mol) and PMDETA (121.1 μL, 0.58 mol) were added via a degassed syringe and the solution was stirred for 30 min in order to form the CuBr/PMDETA complexes. Then followed with the addition of methyl 2-bromopropionate (64.7 μL, 0.58 mol) via a degassed syringe, the reaction mixture was stirred for another 30 min. Note that all of the above processes were operated under nitrogen atmosphere. Next, the flask was immersed in an oil bath at 110 °C to start the polymerization. During the propagation, the system was continually purged with pure nitrogen until the reaction

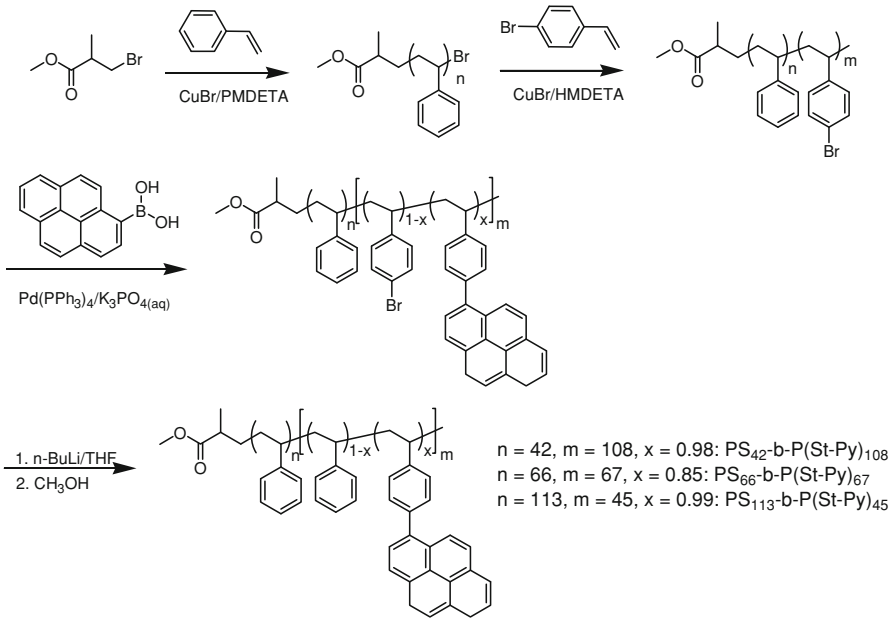

Scheme 1 Synthetic procedures of PS-*b*-P(St-Py) diblock copolymers

was terminated. After 1–2 h, the flask was taken away from the oil bath and opened to atmosphere to terminate the polymerization. After cooling to room temperature, the viscous polymer solution was diluted by adding a small amount of THF. Then, the solution was filtered through a column of neutral aluminum oxide, which was served to remove the copper catalyst from the polymer solution. Afterward, partial THF was removed from the solution by a rotary concentrator. The concentrated solution was further precipitated into methanol twice to remove the styrene monomers. The product, polystyrene macroinitiator (yields: 52%, conversion: 75%) was dried under vacuum overnight. ^{1}H-NMR (CD_2Cl_2): δ (ppm) = 6.4–7.2 (5H, $CH_2CHC_6\underline{H}_5$), 1.3–1.9 (3H, $C\underline{H}_2C\underline{H}C_6H_5$). The number-average molecular weight (M_n) of three different batches of PS-Br macroinitiators estimated from gel permeation chromatography (GPC) are 4390, 6860, and 11840 with the corresponding PDI of 1.34, 1.27, and 1.12, respectively.

Poly(4-bromostyrene) homopolymer (P4BrS)

CuBr (21.94 mg, 0.15 mol) and Me_4cyclam (39.2 mg, 0.15 mol) were added to a Schlenk flask with a magnetic stirring bar and sleeve stoppers. Then, 4-bromostyrene (2 mL, 15.3 mol), methyl 2-bromopropionate (17 μL, 0.15 mol), and anisole (4 mL) were added via a degassed syringe. The mixture was stirred for 30 min in order to form the CuBr/Me_4cyclam complexes. Afterward, the reaction flask was immersed in an oil bath at 110 °C and stirred overnight. The polymerization was stopped by opening the flask and exposing the catalyst to the atmosphere. After cooling to room temperature,

the viscous polymer solution was diluted by a small amount of THF and purified by passing through a column filled with neutral aluminum oxide to remove the copper complex. The eluent was precipitated by pouring the solution into a large excess of methanol to remove the 4-bromostyrene monomers. The product, poly(4-bromostyrene) homopolymer (yields: 50%, conversion: 15%) was dried under vacuum overnight. ^{1}H-NMR (CD_2Cl_2): δ (ppm) = 6.2–7.5 (4H, $CH_2CHC_6\underline{H_4}Br$), 1.2–2.0 (3H, $C\underline{H_2}C\underline{H}C_6H_4Br$). The number-average molecular weight (M_n) and PDI of P4BrS homopolymer are 2720 and 1.32, respectively.

Polystyrene-block-poly(4-bromostyrene) (PS-b-P4BrS)

The macroinitiator, PS-Br (1 g, 0.146 mol), CuBr (20.9 mg, 0.146 mol), and anisole (10 mL) were added to a dry three-neck flask with a magnetic stirring bar and sleeve stoppers. After the PS macroinitiator dissolved, 4-bromostyrene (5.7 mL, 43.8 mol) and HMTETA (39.7 μL, 0.58 mol) were added to the solution via a degassed syringe and then the mixture was stirred for 30 min until the Cu/HMTETA complexes had formed. All the processes were performed under a nitrogen atmosphere. The reaction flask was immersed in an oil bath at 120 °C. After 0.5–2 h, the flask was taken away from the oil bath. The polymerization was terminated by opening the flask and exposing the copper catalyst to the air. After cooling down to room temperature, the viscous polymer solution was diluted by a small amount of THF and passed through a neutral aluminum oxide column to remove the copper catalyst. Then, partial THF was removed from the solution by a rotary concentrator. The concentrated solution was further precipitated into methanol twice to remove the 4-bromostyrene monomers and subsequently precipitated into cyclohexane to remove the unreacted polystyrene macroinitiator. The product, PS-*b*-P4BrS was dried under vacuum at 40 °C overnight in order to obtain PS-*b*-P4BrS diblock as white solid (yields: 55%, conversion: 36%). ^{1}H-NMR (CD_2Cl_2): δ (ppm) = 6.1–7.4 ($CH_2CHC_6\underline{H_5}$, $CH_2CHC_6\underline{H_4}Br$), 1.2–1.7 ($C\underline{H_2}CHC_6H_5$, $C\underline{H_2}CHC_6H_4Br$), 1.7–2.1 ($CH_2C\underline{H}C_6H_5$, $CH_2C\underline{H}C_6H_4Br$). The number-average molecular weight (M_n) of three different batches of PS-*b*-P(4BrS) diblock copolymers estimated from GPC are 21875, 18690, and 19770, respectively, with the corresponding PDI of 1.26, 1.15 and 1.17.

Polystyrene-block-poly(styrene-pyrene) (PS-b-P(St-Py))

A mixture of PS-*b*-P4BrS (400 mg, 0.021 mol), pyrene-1-boronic acid (0.67 g, 4.22 mol), $Pd(PPh_3)_4$ (16.2 mg, 0.014 mol) and five drops of Aliquat® 336 were dissolved in anhydrous THF (15 mL) and 2.0 M K_3PO_4 aqueous (10 mL) solution. The reaction flask was immersed in an oil bath at 85 °C and the reaction mixture was kept under reflux for 3 days. Then, partial THF was removed from the polymer solution by rotary concentrator. The polymer was purified by washing with methanol and then dried under vacuum at 40 °C overnight. In order to remove the unreacted bromide of the P(St-Py) block, we focused on Br–Li exchange reaction [46]. The PS-*b*-P(St-Py) diblock copolymer (300 mg, 0.013 mol), THF (5 mL), and 1.1 equiv. of a hexane solution of *n*-BuLi (270 μL, 0.27 mol) were added in the

round-bottomed flask at −78 °C stirring for 1 h. Then, followed with the adding of methanol (1 mL) and stirred for 10 min. Finally, the mixture was diluted by a little of THF and precipitated into excess amount of methanol, filtered out, and dried under vacuum at 40 °C overnight to obtain PS-*b*-P(St-Py) (yield: 55%). ^{1}H-NMR (CD_2Cl_2): δ (ppm) = 7.5–8.2 (protons on pyrene group), 6.3–7.5 (protons on phenyl group), 1.2–2.0 ($C\underline{H_2}C\underline{H}C_6H_5$, $C\underline{H_2}C\underline{H}C_6H_4$). The number-average molecular weight (M_n) of three different batches of PS-*b*-P(St-Py) diblock copolymers estimated from GPC are 34065, 25330, and 28620, respectively, with the corresponding PDI of 1.28, 1.14, and 1.21.

Poly(styrene-pyrene) homopolymer (P(St-Py))

A mixture of P4BrS (300 mg, 0.11 mol), pyrene-1-boronic acid (1.22 g, 4.96 mol), $Pd(PPh_3)_4$ (20 mg, 0.017 mol), and three drops of Aliquat® 336 were dissolved in anhydrous THF (15 mL) and 2.0 M K_3PO_4 aqueous (10 mL) solution. The reaction flask was immersed in an oil bath at 85 °C and the reaction mixture was kept under reflux for 3 days. Afterward, the homopolymer was purified by washing with methanol in order to remove the excess boronic acid and then dried under vacuum at 40 °C overnight. ^{1}H-NMR (CD_2Cl_2): δ (ppm) = 7.5–8.2 (9H, protons on pyrene group), 6.3–7.5 (4H, protons on phenyl group), 1.2–2.0 (3H, $C\underline{H_2}C\underline{H}C_6H_4$). The number-average molecular weight (M_n) and PDI of P(St-Py) homopolymer are 3,300 and 1.36, respectively.

Characterization

Molecular weight distribution was determined by GPC using a Lab Alliance RI2000 instrument (PLgel 5 μm MIXED-D from Polymer Laboratories) connected with one refractive index detector from Schambeck SFD Gmbh. All GPC analyses were performed on polymer/THF solutions at a flow rate of 1 mL/min at 40 °C and calibrated with polystyrene. ^{1}H-NMR spectra were recorded at room temperature on a Bruker AM 400 (400 MHz) spectrometer using the residual proton resonance of the deuterated dichloromethane as the internal standard. Thermal analyses were carried out on a thermogravimetric analyzer (TGA) from TA Q50 with heating range from 100 to 800 °C at the heating rate of 10 °C/min and a differential scanning calorimetry (DSC) from TA instrument (TA Q100) with heating cycle from −30 to 300 °C at the heating rate of 5 °C/min.

UV–Vis absorption and photoluminescence (PL) spectra were recorded with UV–VIS-NIR spectrophotometer (Hitachi, U4100) and Fluorolog-3 spectrofluorometer (Jobin Yvon), respectively. Cyclic voltammetry (CV) was performed with the use of a three-electrode cell in which ITO (polymer films area about 0.7×0.5 cm^2) was used as a working electrode. A platinum wire was used as an auxiliary electrode. All cell potentials were taken with the use of a homemade Ag/AgCl, KCl (sat.) reference electrode.

The thickness of the polymer film was measured with a Microfigure Measuring Instrument (Surfcorder ET3000, Kosaka Laboratory Ltd). Atomic force micrographs of the polymer films on device surface were obtained with a Nanoscope 3D

Controller AFM (Digital Instruments, Santa Barbara, CA) operated in the tapping mode at room temperature. Commercial silicon cantilevers (Nanosensors, Germany) with typical spring constants 21–78 Nm^{-1} was used and the images were taken continuously with the scan rate of 1.0 Hz.

Fabrication and characterization of the memory devices

The memory devices were fabricated on the indium tin oxide (ITO)-coated glass, with the configuration of ITO/Polymer/Al expressed in Fig. 1. Before the fabrication of the polymer layer, the glass was pre-cleaned by ultrasonication with water, isopropanol, and acetone each for 15 min, respectively. Afterward, 8 mg/mL of polymer solution in chloroform was first filtered through 0.45-μm pore size of PTFE membrane syringe filter. Then, the filtered solution was spin-coated onto the pre-cleaned ITO glass at a speed rate of 800 rpm for 60 s and baked at 80 °C for 10 min under vacuum. The polymer film thickness from chloroform solution was around 60 nm. Finally, a 200-nm thick Al top electrode (recorded device units of 0.5 × 0.5 mm^2 in size) was thermally evaporated through the shadow mask at a pressure of 10^{-7} torr with a uniform depositing rate of 3–5 Å/s. The electrical characterization of the memory device was performed by a Keithley 4200-SCS semiconductor parameter analyzer equipped with a Keithely 4205-PG2 arbitrary waveform pulse generator. ITO was used as the cathode and Al was set as the anode during the voltage sweep with a step of 0.1 V. The probe tip used 10-μm diameter tungsten wire attached to a tinned copper shaft with a point radius <0.1 μm (GGB Industries, Inc.). All of the electronic measurements were performed at room temperature in a glove box.

Results and discussion

Synthesis and thermal properties of PS-*b*-P(St-Py) diblock copolymers

Three PS_n-*b*-$P(St\text{-}Py)_m$ diblock copolymers with different block ratios were synthesized to investigate the effect of the pyrene content on the optoelectronic

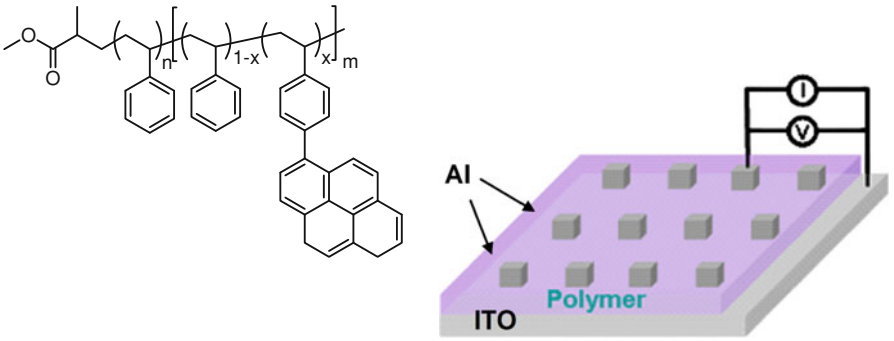

Fig. 1 Geometries of the ITO/polymer/Al memory device

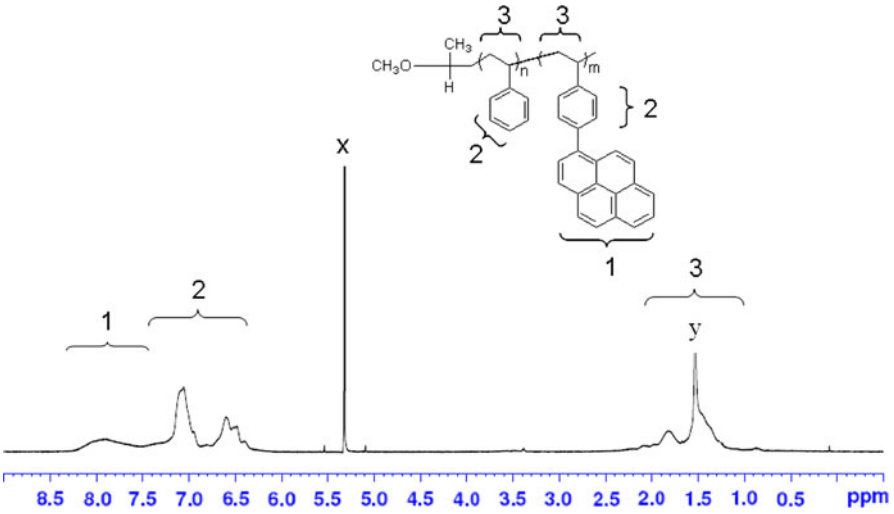

Fig. 2 ^{1}H-NMR spectra of PS_{113}-*b*-$P(St\text{-}Py)_{45}$ in CD_2Cl_2. (*x*: CD_2Cl_2, *y*: H_2O)

properties of the copolymers. Figure 2 shows the ^{1}H-NMR spectrum of PS_{113}-*b*-$P(St\text{-}Py)_{45}$ in CD_2Cl_2. The proton peaks at 7.5–8.2 ppm are assigned to the characteristic peaks of pyrene group. The phenyl and alkyl proton signals contributed by the polystyrene moieties are observed around 7.5–6.3 and 1.2–2.0 ppm, respectively. The ^{1}H-NMR spectra of PS_{42}-*b*-$P(St\text{-}Py)_{108}$ and PS_{66}-*b*-$P(St\text{-}Py)_{67}$ listed in the supporting information are also consistent with the proposed structure. The above results revealed the successful preparation of PS-*b*-P(St-Py).

The molecular weights of PS-Br, P4BrS, P(St-Py), PS-*b*-P(St-4BrS), and PS-*b*-P(St-Py) were estimated by GPC analysis. The number-average molecular weight (M_n) of the three PS-*b*-P(St-Py) diblock copolymers are 34065, 25330, and 28620 with the corresponding PDI of 1.28, 1.14, and 1.21, respectively. The block length (*n* and *m*) in PS_n-*b*-$P(St\text{-}Py)_m$ were determined in the following procedure. First, the molecular weight and DP of PS-Br macroinitiator (*n*) were estimated by GPC since it was calibrated with polystyrene standard. Then, the block ratio (*n*/*m*) of copolymers was determined by the ^{1}H-NMR spectra through the peak ratios of pyrene and phenyl proton. In the following, the DP of P(St-Py) block (*m*) was estimated by subtracting the M_n of PS-*b*-P(St-Py) from that of the PS block. The block ratios of the three different diblock copolymers are thus obtained to be PS_{42}-*b*-$P(St\text{-}Py)_{108}$, PS_{66}-*b*-$P(St\text{-}Py)_{52}$, and PS_{113}-*b*-$P(St\text{-}Py)_{45}$, respectively. The degree of substitution (*x* in Scheme 1) of bromide with pyrene was estimated by comparing the ^{1}H-NMR spectra of PS-*b*-P(St-Py) with those of corresponding PS-*b*-P(4BrS). The values of degree of substitution for PS_{42}-*b*-$P(St\text{-}Py)_{108}$, PS_{66}-*b*-$P(St\text{-}Py)_{52}$, and PS_{113}-*b*-$P(St\text{-}Py)_{45}$ are 98, 85, and 99%, respectively. These high values for the degree of substitution suggest the successful replacement of bromide with pyrene as we proposed.

All the polymers were readily soluble in common organic solvents such as tetrahydrofuran (THF), chloroform, and dichloromethane. Thermogravimetric analysis (TGA) was used to determine the thermal stability of these pendant pyrene moieties diblock copolymers [refer online resource Fig. S2(a)]. A 5% weight loss is defined as the thermal decomposition temperature (T_d). The T_d values of PS_{42}-*b*-$P(St\text{-}Py)_{108}$, PS_{66}-*b*-$P(St\text{-}Py)_{67}$, and PS_{113}-*b*-$P(St\text{-}Py)_{45}$ are observed at 352, 349, and 353 °C, respectively. The glass transition temperature (T_g) of all the studied polymers were estimated from DSC [refer online resource Fig. S2(b)]. The T_g values of the aforementioned three copolymers from the DSC curves are found at 163.9, 119.7, and 102.3 °C, respectively. The observation of only one glass transition temperature for PS-*b*-P(St-Py) instead of two T_g from each block suggests that the PS block and P(St-Py) block are highly miscible without microphase separation. The T_d of all the diblock copolymers are higher than 350 °C, indicative of good thermal stability for electrical device applications.

Optical properties

Figure 3 shows the UV–Vis and PL spectra of PS-*b*-P(St-Py) diblock copolymers in dilute chloroform solution and thin films. The corresponding optical properties of these three copolymers are summarized in Table 1. As shown in Fig. 3a, the optical absorption peak maxima (λ_{max}^{abs}) of the three PS-*b*-P(St-Py) copolymers in chloroform solutions are observed identically. However, the corresponding PL spectra show a slight blue shift (from 461 to 457 nm) with decreasing pyrene content, which is probably attributed the interactions between the pyrene moiety. PS_{42}-*b*-$P(St\text{-}Py)_{108}$ and PS_{66}-*b*-$P(St\text{-}Py)_{67}$ with higher pyrene contents may have different conjugated length distributions and lead to broader PL spectra than PS_{113}-*b*-$P(St\text{-}Py)_{45}$. As observed in Fig. 3(b), λ_{max}^{abs} of PS_{42}-*b*-$P(St\text{-}Py)_{108}$ spin-coated film is at 352 nm, which is attributed to the π–π interaction of the P(St-Py) block. However, for PS_{113}-*b*-$P(St\text{-}Py)_{45}$ film with less pyrene content, a hypsochromic (blue) shift of the λ_{max}^{abs} (from 352 to 349 nm) is observed. The emission maximums (λ_{max}^{PL}) of PS_{42}-*b*-$P(St\text{-}Py)_{108}$, PS_{66}-*b*-$P(St\text{-}Py)_{67}$, and PS_{113}-*b*-$P(St\text{-}Py)_{45}$ spin-coated films are exhibited at the wavelength 457, 453, and 440 nm, respectively. The above photophysical properties suggest that the long PS block may inhibit the strong π–π interaction of the pyrene moieties and reduce its effective conjugated length. The optical band gaps of PS_{42}-*b*-$P(St\text{-}Py)_{108}$, PS_{66}-*b*-$P(St\text{-}Py)_{67}$, and PS_{113}-*b*-$P(St\text{-}Py)_{45}$ spin-coated films estimated from the onset optical absorbance are 3.18, 3.14, and 3.16 eV, respectively.

Electrochemical properties

The electrochemical properties of these three copolymers were investigated by CV, using the spin-coated film on an ITO-coated glass substrate as working electrode in anhydrous acetonitrile containing 0.1 M of TBAP as electrolyte under nitrogen atmosphere. The HOMO energy levels of the prepared polymers were calculated with the onset voltage of oxidation peaks with reference to ferrocene (4.8 eV) by the following equation: $\text{HOMO} = -\text{e}\,(E_{onset}^{ox} - E_{ferrocene}^{1/2} + 4.8)$ (eV). The lowest

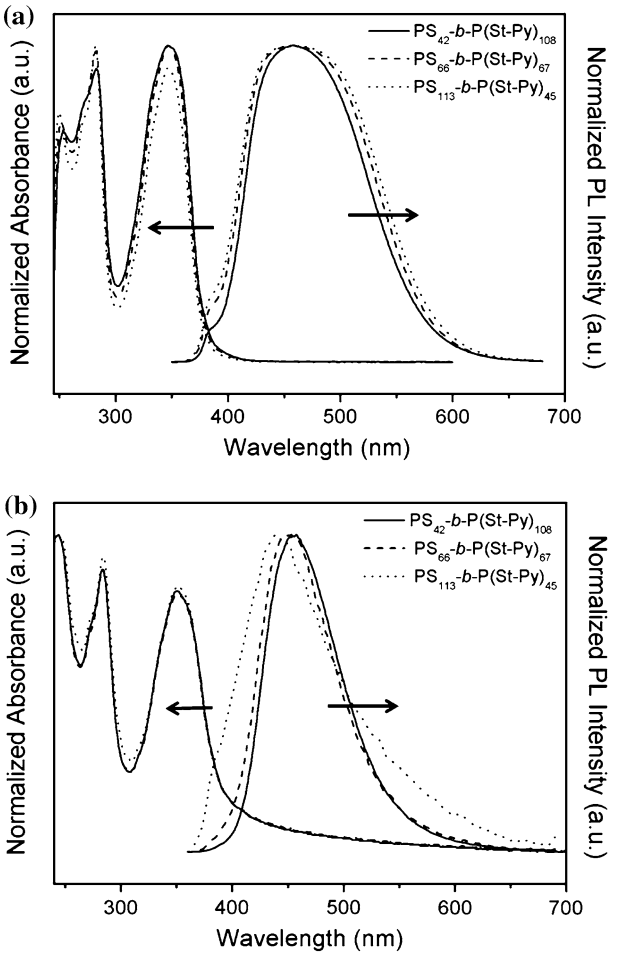

Fig. 3 UV-vis absorption and PL spectra of PS_{42}-*b*-P(St-Py)$_{108}$, PS_{66}-*b*-P(St-Py)$_{67}$, and PS_{113}-*b*-P(St-Py)$_{45}$ in **a** chloroform and **b** thin films spin coated from chloroform

Table 1 Optical and electrochemical properties of the PS-*b*-P(St-Py) diblock copolymers

Entry	λ_{max}^{abs} (nm) Soln	λ_{max}^{abs} (nm) Film	λ_{max}^{PL} (nm) Slon	λ_{max}^{PL} (nm) Film	E_g^{opt} (eV)	E_{onset}^{ox} (V)	HOMO (eV)	LUMO (eV)
PS_{42}-*b*-P(St-Py)$_{108}$	347	352	461	457	3.18	1.31	−5.62	−2.44
PS_{66}-*b*-P(St-Py)$_{67}$	347	350	459	453	3.14	1.36	−5.67	−2.53
PS_{113}-*b*-P(St-Py)$_{45}$	346	349	457	440	3.16	1.41	−5.72	−2.56

unoccupied molecular orbital (LUMO) level was calculated with HOMO and the value of the optical band gap (E_g^{opt}) according to the relation LUMO = HOMO + E_g^{opt} (eV) [22]. Figure 4 represents the cyclic voltammograms of these three

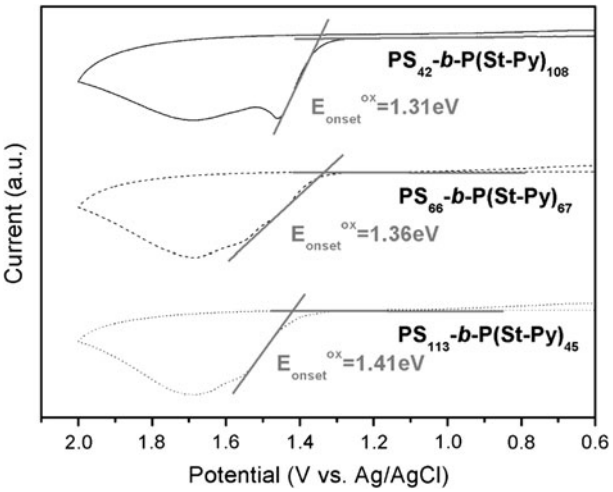

Fig. 4 Cyclic voltammograms of PS_{42}-*b*-P(St-Py)$_{108}$, PS_{66}-*b*-P(St-Py)$_{67}$, and PS_{113}-*b*-P(St-Py)$_{45}$ thin films spin-coated onto ITO glass

copolymers, and the corresponding electrochemical properties are given in Table 1. From the measurement of CV, the HOMO energy levels of PS_{42}-*b*-P(St-Py)$_{108}$, PS_{66}-*b*-P(St-Py)$_{67}$, and PS_{113}-*b*-P(St-Py)$_{45}$ are estimated to be −5.62, −5.67, and −5.72 eV, respectively. This suggests that the HOMO level is enhanced with an increase in the effective conjugated length of the pendant pyrene groups. On the other hand, the LUMO energy levels of PS_{42}-*b*-P(St-Py)$_{108}$, PS_{66}-*b*-P(St-Py)$_{67}$, and PS_{113}-*b*-P(St-Py)$_{45}$ are to be −2.44, −2.53, and −2.56 eV, respectively, which are estimated from the difference between the HOMO level and optical band gap. The energy levels of the prepared polymers lead to different memory characteristics, as discussed in the following.

Performance of the memory device

The effect of the pyrene content in PS-*b*-P(St-Py) on the performance of memory device was investigated using the ITO/polymer/Al device structure of Fig. 1. Al was used as the anode and ITO was set as the cathode in all electrical measurements. All the thickness of active memory films was adjusted to be around 60 nm. The smooth root-mean-square surface roughness of the PS-*b*-P(St-Py) films estimated from AFM is 0.7–0.9 nm (refer online resource Fig. S3). Also, there is no ordered structure for the block copolymer films, probably due to the large side group. It indicates the surface structure of the PS-*b*-P(St-Py) would not play an significant role on the memory characteristics.

The current–voltage (*I*–*V*) characteristic of PS_{42}-*b*-P(St-Py)$_{108}$ is shown in Fig. 5a. In the first sweep from 0 to −5 V, an abrupt increase in current is observed at a switching threshold voltage of about −2.7 V, indicating the device transition from a low-conductivity (OFF) state to a high-conductivity (ON) state (the "writing" process). The device remains in this high-conductivity state during the

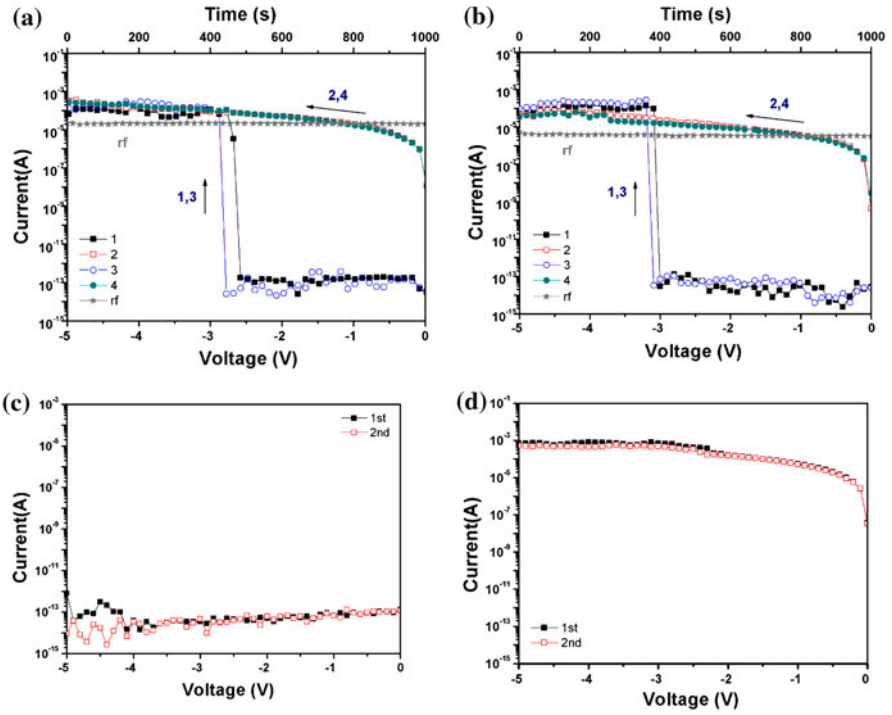

Fig. 5 Current–voltage (*I–V*) characteristics of the **a** PS_{42}-*b*-$P(St\text{-}Py)_{108}$, **b** PS_{66}-*b*-$P(St\text{-}Py)_{67}$, **c** PS_{113}-*b*-$P(St\text{-}Py)_{45}$, and **d** $P(St\text{-}Py)_{15}$ memory device

subsequent negative scan (the second sweep). The distinct bielectrical states in the voltage range of 0 to −2.7 V allow a voltage to read the "0" or "OFF" signal and "1" or "ON" signal of the memory. Subsequent application of the third scan performed after turning off power for about 3 min can be reprogrammed from the OFF state to ON state at −2.7 V again and the current is kept in the ON state. It can be seen that an ON/OFF current ratio of 10^9 is obtained. The OFF state can be further written to the ON state when the switching threshold voltage is reapplied, indicating that the memory device is rewritable. The short retention time of the ON state suggests that the memory device is volatile. This behavior is characteristic of a dynamic random access memory (DRAM) device. The unstable ON state is electrically sustained by a refreshing voltage pulse of −1 V in every 5 s (the rf trace in Fig. 5a).

Likewise, the memory effect of PS_{66}-*b*-$P(St\text{-}Py)_{67}$ is shown in the current–voltage (*I–V*) characteristic of Fig. 5b. Similarly, the *I–V* characteristic defines the two electrical conductance states of PS_{66}-*b*-$P(St\text{-}Py)_{67}$ device and reveal the volatile nature of the memory effect. This memory device switches from the OFF to ON state at about −3.1 V, with an ON/OFF current ratio of about 10^9, when a voltage sweep from 0 to −5 V is applied. The device remains in the ON state when the voltage sweep is repeated. Also, it is able to keep in the ON state for a period of

3 min after turning off the power. After turning off the power for more than 3 min, the device drops back to the OFF state but can be switched ON again by applying the appropriate voltage (the third sweep). Thus, the behavior of this memory device shows the common characteristics of a DRAM. In addition, the ON state can be electrically sustained by refreshing pulses of −1 V every 5 s, as seen in Fig. 5b.

On the other hand, for the lower pyrene content, the *I–V* curve of the PS_{113}-*b*-$P(St\text{-}Py)_{45}$ device display an insulating state in a low current variation of 10^{-12} to 10^{-14} A, as shown in Fig. 5c. In addition, the devices based on the corresponding homopolymers, PS and P(St-Py), were also characterized for reference. A PS homopolymer shows a low current ($<10^{-8}$ A) even with an increase in the applied voltage. This suggests that the PS-based device acts as an insulator without any memory effect [25, 37]. Whereas the device with P(St-Py) as the active polymer layer shows it to be constantly in a single high-conductivity state, and no conductance switching behavior is observed when the voltage across the device is swept from 0 to −5 V, as shown in Fig. 5d.

Figure 6 shows the retention time tests under a constant stress of −1 V for both the ON and OFF states of PS_{42}-*b*-$P(St\text{-}Py)_{108}$ and PS_{66}-*b*-$P(St\text{-}Py)_{67}$, respectively. At a constant stress of −1 V, no obvious change in the current for the OFF and ON state is observed during the long-term testing in a glove box, which suggests the excellent device stability. In addition, the stimulus effect of continuous read pulse with a read voltage of −1 V in the ON and OFF state was also investigated as shown in Fig. 7. The inset in Fig. 7 shows the pulse generation used in the measurement with a pulse period of 1 μs and width of 1 μs. Both the ON and OFF states are also stable up to 10^8 read cycles at a read voltage of −1 V. No resistance degradation is observed for both the ON and OFF states during the measurement. Hence, both ON and OFF states are conducted under the voltage stress and are insensitive to continuous pulse cycles.

Mechanism of the memory device

To understand the observed memory characteristics, the HOMO and LUMO levels of these three diblock copolymers, those levels of P(St-Py) homopolymers and the work functions of the aluminum (−4.28 eV) top and ITO (−4.8 eV) bottom electrodes are considered. The relative energy diagram is summarized in Fig. 8. With a configuration of ITO/PS-*b*-P(St-Py)/Al device, the energy barrier between the work functions of the ITO bottom electrode and the HOMO level of the active polymer layer is 0.82–0.92 eV, which is much smaller than that (1.72–1.84 eV) between the LUMO level of the active polymer layer and the work function of the Al top electrode. Thus, the hole injection from the ITO bottom electrode into the HOMO level of the polymer layer is much more favorable than the electron injection from the Al top electrode into the LUMO level of the polymer layer. Therefore, the hole injection dominates the conduction process in the devices. In addition, P(St-Py) homopolymer has a higher HOMO energy level (−5.56 eV) than that of the PS_n-*b*-$P(St\text{-}Py)_m$ diblock copolymers (−5.62 to −5.72 eV) and thus can serve as a hole-transporting moiety. However, the insulating characteristic of polystyrene moieties embedded in the polymer thin film layer would serve as the

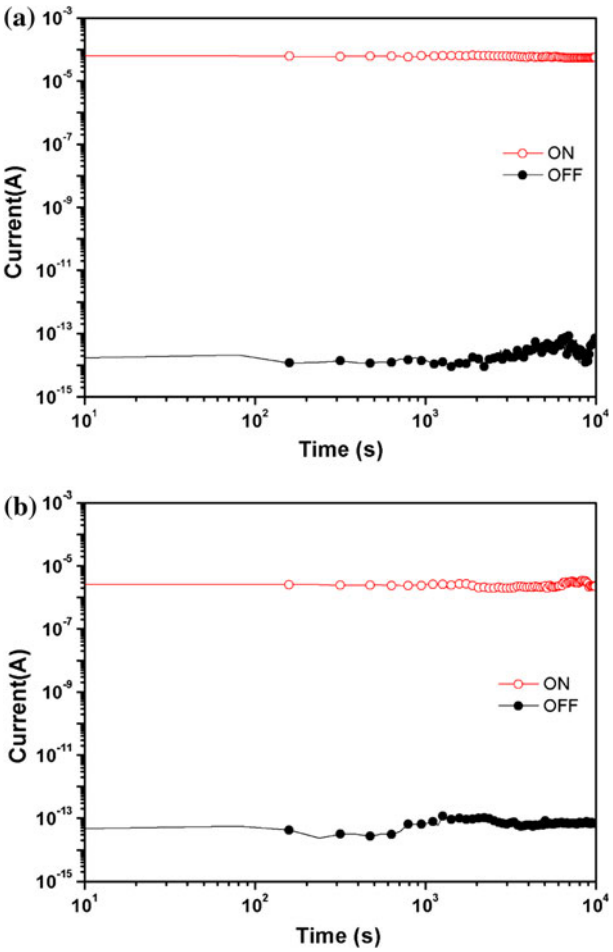

Fig. 6 Retention time test in the ON and OFF states of the **a** PS_{42}-*b*-$P(St\text{-}Py)_{108}$ and **b** PS_{66}-*b*-$P(St\text{-}Py)_{67}$ device under a continuous readout voltage

hole-blocking domain in the active memory layer. For the case of the highest polystyrene content in these three copolymers, the *I–V* characteristic curve of PS_{113}-*b*-$P(St\text{-}Py)_{45}$ device shown in Fig. 5c exhibits a low current state between 10^{-12} and 10^{-14} A and suggests its insulating characteristic, similar to that reported in the literature [25, 37]. On the other hand, the P(St-Py) hole-transporting moiety provides the hole hoping with neighboring pyrene unit under the electric field and contributes to the ON state conductance. Therefore, the threshold voltage for electrical switching between the top and bottom electrodes might depends on the P(St-Py) content of the diblock copolymers. The larger amount of holes accumulated in the P(St-Py) under higher voltage might help the hopping of charge carriers across the hole-blocking polystyrene domain. On the other hand, the

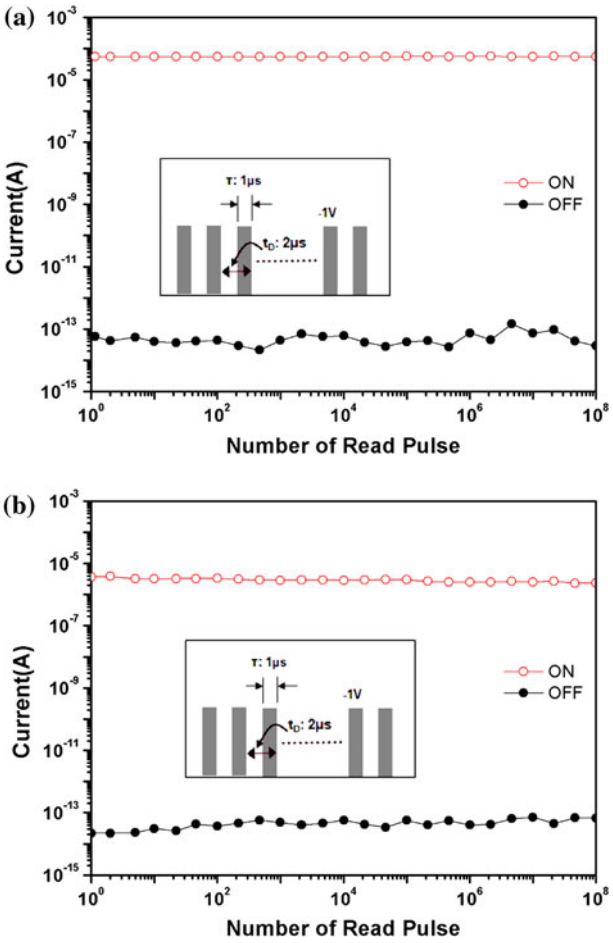

Fig. 7 Stimulus effect of read pulses in the ON and OFF states of the **a** PS_{42}-*b*-$P(St\text{-}Py)_{108}$ and **b** PS_{66}-*b*-$P(St\text{-}Py)_{67}$ devices. The *inset* shows the pulse shapes in the measurement

higher polystyrene ratio of diblock copolymers may prevent the positive charge from direct hopping process and the device could still be kept in the OFF state.

For the case of device with a higher pyrene content, PS_{42}-*b*-$P(St\text{-}Py)_{108}$ and PS_{66}-*b*-$P(St\text{-}Py)_{67}$, the electrical switching exhibits the volatile memory behavior. Under a low voltage bias, holes do not have sufficient energy to overcome the energy barrier between styrene/pyrene moieties and are blocked by the polystyrene moieties in the film. Thus, the device is on the low conductance (OFF) state. As sweeping up to the threshold voltage, the amounts of holes accumulated with sufficient activation energy to hop across the polystyrene moieties. The holes are able to flow continuously and more effectively in the copolymers film, switching the device from the OFF to ON state. The increase of current is probably resulted from the efficient interchain hopping of the charge carriers in the neighboring pyrene chain. The ON state cannot be maintained without a continuous voltage bias and it

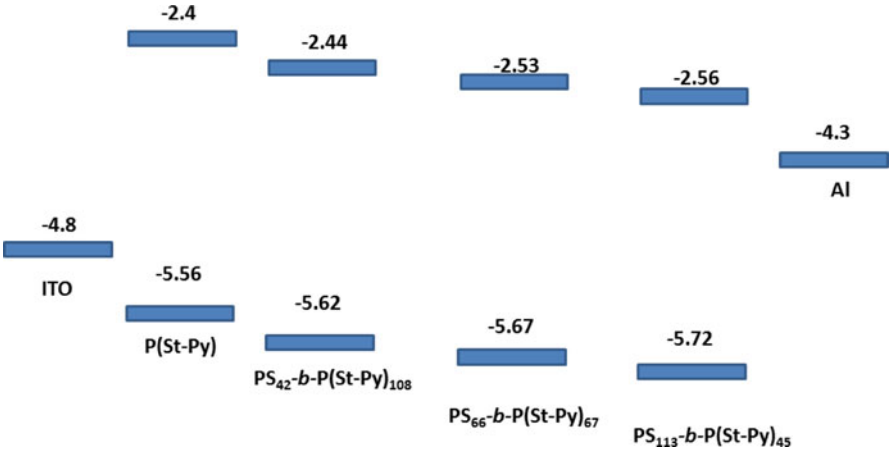

Fig. 8 Molecular simulation of HOMO and LUMO energy levels for PS_n-*b*-$P(St\text{-}Py)_m$ along with the work function of the electrodes

returns to the original state after the removal of the applied electric field for a short period of time. This is probably due to the shallow depth of trap. The shallow traps contribute to the possible back transferring of trapped charge and thus result in the unstable ON state of the volatile nature. In addition, the smaller threshold voltage and higher current ratio of PS_{42}-*b*-$P(St\text{-}Py)_{108}$ as compared with PS_{66}-*b*-$P(St\text{-}Py)_{67}$ may be attributed to the lower hole injection barrier between ITO/polymer interface. It concludes that electric-field-induced memory switching behaviors based on PS_{42}-*b*-$P(St\text{-}Py)_{108}$ and PS_{66}-*b*-$P(St\text{-}Py)_{67}$ diblock copolymers depend on the charge hopping conduction between the pyrene units with coexisting charge-trapping environment and the volatility of the memory effect is determined from the ability of charge trapping/back transferring of trapped charge.

The prepared block copolymers could not have an ordered morphology to study the morphological effect on the electrical memory characteristics, which is probably due to the large side group. However, it is expected that block polymer with ordered morphology could be prepared by the simple and versatile synthetic scheme in this study and used for controlling electrical memory characteristics.

Conclusions

We have successfully synthesized the new non-conjugated diblock copolymers containing pendant pyrene moieties by combining ATRP and Suzuki coupling reaction. The insulating characteristics of polystyrene could be served as hole-blocking moieties and provide the charge-trapping environment. Thus, the pendant pyrene-based polymers exhibited the electrical volatile nature, which was attributed to the back transferring of shallow trapped charges in the pendant pyrene groups. The memory devices with a higher pyrene content showed the DRAM memory devices, which were electrically stable for at least 10^4 s under a constant voltage

stress. They could endure 10^8 cycles under a pulse read voltage in both ON and OFF state. Also, the polymers with a higher pyrene content enhanced the HOMO level and thus reduced the turn-on threshold voltage. Our results provided the strategies to manipulate the memory characteristics with pendant pyrene content in functional polymers.

Acknowledgments This research work is supported by the National Science Council and the Ministry of Economic Affairs of Taiwan.

References

1. Scott JC, Bozano LD (2007) Nonvolatile memory elements based on organic materials. Adv Mater 19:1452–1463
2. Osaka T, Takai M, Hayashi K, Ohashi K, Saito M, Yamada K (1998) A soft magnetic CoNiFe film with high saturation magnetic flux density and low coercivity. Nature 392:796–798
3. Kawata S, Kawata Y (2000) Three-dimensional optical data storage using photochromic materials. Chem Rev 100:1777–1788
4. Hagen R, Bieringer T (2001) Photoaddressable polymers for optical data storage. Adv Mater 13:1805–1810
5. Möller S, Perlov C, Jackson W, Taussig C, Forrest SR (2003) A polymer/semiconductor write-once read-many-times memory. Nature 426:166–169
6. Rozenberg MJ, Inoue IH, Sanchez MJ (2004) Nonvolatile memory with multilevel switching: a basic model. Phys Rev Lett 92:178302
7. Wang J-P (2005) Magnetic Data Storage Tilting for the top. Nat Mater 4:191–192
8. Kapetanakis E, Douvas AM, Velessiotis D, Makarona E, Argitis P, Glezos N, Normand P (2008) Molecular storage elements for proton memory devices. Adv Mater 20:4568–4574
9. Ling QD, Liaw DJ, Zhu C, Chan DSH, Kang ET, Neoh KG (2008) Polymer electronic memories: materials, devices and mechanisms. Prog Polym Sci 33:917–978
10. Li H, Xu Q, Li N, Sun R, Ge J, Lu J, Gu H, Yan F (2010) A small-molecule-based ternary data-storage device. J Am Chem Soc 132:5542–5543
11. Yang Y, Ouyang J, Ma L, Tseng RJH, Chu CW (2006) Electrical switching and bistability in organic/polymeric thin films and memory devices. Adv Funct Mater 16:1001–1014
12. Chen J, Ma D (2005) Single-layer organic memory devices based on *N*,*N*′-di(naphthalene-l-yl)-*N*,*N*′-diphenyl-benzidine. Appl Phys Lett 87:023505
13. Lin J, Ma D (2008) The morphology control of pentacene for write-once-read-many-times memory devices. J Appl Phys 103:024507
14. Tu CH, Lai YS, Kwong DL (2006) Memory effect in the current–voltage characteristic of 8-hydroquinoline aluminum salt films. IEEE Electron Device Lett 27:354–356
15. Ouisse T, Stéphan O (2004) Electrical bistability of polyfluorene devices. Org Electron 5:251–256
16. Ling QD, Song Y, Lim SL, Teo EYH, Tan YP, Zhu C, Chan DSH, Kwong DL, Kang ET, Neoh KG (2006) A dynamic random access memory based on a conjugated copolymer containing electron-donor and -acceptor moieties. Angew Chem Int Ed 45:2947–2951
17. Baek S, Lee D, Kim J, Hong SH, Kim O, Ree M (2007) Novel digital nonvolatile memory devices based on semiconducting polymer thin films. Adv Funct Mater 17:2637–2644
18. Kim TW, Oh SH, Choi H, Wang G, Hwang H, Kim D-Y, Lee T (2008) Reversible switching characteristics of polyfluorene-derivative single layer film for nonvolatile memory devices. Appl Phys Lett 92:253308
19. Lee TJ, Park S, Hahm SG, Kim DM, Kim K, Kim J, Kwon W, Kim Y, Chang T, Ree M (2009) Programmable digital memory characteristics of nanoscale thin films of a fully conjugated polymer. J Phys Chem C 113:3855–3861
20. Ling QD, Chang FC, Song Y, Zhu CX, Liaw DJ, Chan DSH, Kang ET, Neoh KG (2006) Synthesis and dynamic random access memory behavior of a functional polyimide. J Am Chem Soc 128:8732–8733

21. Lee TJ, Chang C-W, Hahm SG, Kim K, Park S, Kim DM, Kim J, Kwon W-S, Liou G-S, Ree M (2009) Programmable digital memory devices based on nanoscale thin films of a thermally dimensionally stable polyimide. Nanotechnology 20:135204
22. You NH, Chueh CC, Liu CL, Ueda M, Chen WC (2009) Synthesis and memory device characteristics of new sulfur donor containing polyimides. Macromolecules 42:4456–4463
23. Hahm SG, Choi S, Hong SH, Lee TJ, Park S, Kim DM, Kwon WS, Kim K, Kim O, Ree M (2008) Novel rewritable, non-volatile memory devices based on thermally and dimensionally stable polyimide thin films. Adv Funct Mater 18:3276–3282
24. Hahm SG, Choi S, Hong SH, Lee TJ, Park S, Kim DM, Kim JC, Kwon W, Kim K, Kim MJ, Kim O, Ree M (2009) Electrically bistable nonvolatile switching devices fabricated with a high performance polyimide bearing diphenylcarbamyl moieties. J Mater Chem 19:2207–2214
25. Huang CM, Liu YS, Chen CC, Wei KH, Sheu JT (2008) Electrical bistable memory device based on a poly(styrene-*b*-4-vinylpyridine) nanostructured diblock copolymer thin film. Appl Phys Lett 93: 203303
26. Jian L, Dongge M (2008) Realization of write-once-read-many-times memory devices based on poly(*N*-vinylcarbazole) by thermally annealing. Appl Phys Lett 93:093505
27. Lai YS, Tu CH, Kwong DL, Chen JS (2006) Charge-transport characteristics in bistable resistive poly(*N*-vinylcarbazole) films. IEEE Electron Device Lett 27:451–453
28. Lai YS, Tu CH, Kwong DL, Chen JS (2005) Bistable resistance switching of poly(*N*-vinylcarbazole) films for nonvolatile memory applications. Appl Phys Lett 87:122101
29. Ling QD, Lim SL, Song Y, Zhu CX, Chan DSH, Kang ET, Neoh KG (2006) Nonvolatile polymer memory device based on bistable electrical switching in a thin film of poly(*N*-vinylcarbazole) with covalently bonded C60. Langmuir 23:312–319
30. Teo EYH, Ling QD, Song Y, Tan YP, Wang W, Kang ET, Chan DSH, Zhu C (2006) Non-volatile WORM memory device based on an acrylate polymer with electron donating carbazole pendant groups. Org Electron 7:173–180
31. Ouyang J, Chu CW, Szmanda CR, Ma L, Yang Y (2004) Programmable polymer thin film and nonvolatile memory device. Nat Mater 3:918–922
32. Tseng RJ, Baker CO, Shedd B, Huang J, Kaner RB, Ouyang J, Yang Y (2007) Charge transfer effect in the polyaniline-gold nanoparticle memory system. Appl Phys Lett 90:053101
33. Lin HT, Pei Z, Chen YJ (2007) Carrier transport mechanism in a nanoparticle-incorporated organic bistable memory device. IEEE Electron Device Lett 28:569–571
34. Kanwal A, Chhowalla M (2006) Stable, three layered organic memory devices from C60 molecules and insulating polymers. Appl Phys Lett 89:203103
35. Laiho A, Majumdar HS, Baral JK, Jansson F, Osterbacka R, Ikkala O (2008) Tuning the electrical switching of polymer/fullerene nanocomposite thin film devices by control of morphology. Appl Phys Lett 93:203309
36. Majumdar HS, Baral JK, Österbacka R, Ikkala O, Stubb H (2005) Fullerene-based bistable devices and associated negative differential resistance effect. Org Electron 6:188–192
37. Baral JK, Majumdar HS, Laiho A, Jiang H, Kauppinen EI, Ras RHA, Ruokolainen J, Ikkala O, Osterbacka R (2008) Organic memory using [6, 6]-phenyl-C61 butyric acid methyl ester: morphology, thickness and concentration dependence studies. Nanotechnology 19:035203
38. Lim SL, Ling Q, Teo EYH, Zhu CX, Chan DSH, Kang ET, Neoh KG (2007) Conformation-induced electrical bistability in non-conjugated polymers with pendant carbazole moieties. Chem Mater 19:5148–5157
39. Fang YK, Liu CL, Chen WC (2011) New random copolymers with pendant carbazole donor and 1,3,4-oxadiazole acceptor for high performance memory device applications. J Mater Chem 21: 4778–4786
40. Fang YK, Liu CL, Yang GY, Chen PC, Chen WC (2011) New donor-acceptor random copolymers with pendant triphenylamine and 1,3,4-oxadiazole for high performance memory device applications. Macromolecules 44:2604–2612
41. Liu CL, Hsu JC, Chen WC, Sugiyama K, Hirao A (2009) Non-volatile memory devices based on poly(styrene) derivatives with electron-donating oligofluorene pendant moieties. ACS Appl Mater Interface 1:1974–1979
42. Yun C, You J, Kim J, Huh J, Kim E (2009) Photochromic fluorescence switching from diarylethenes and its applications. J Photochem Photobiol C 10:111–129
43. Yoo J, Kwon T, Sarwade BD, Kim Y, Kim E (2007) Multistate fluorescence switching of *s*-triazine-bridged *p*-phenylene vinylene polymers. Appl Phys Lett 91:241107

44. Kim Y, Kim E, Clavier G, Audebert P (2006) New tetrazine-based fluoroelectrochromic window; modulation of the fluorescence through applied potential. Chem Commun 3612–3614
45. You J, Heo JS, Lee J, Kim HS, Kim HO, Kim E (2009) A fluorescent polymer for patterning of mesenchymal stem cells. Macromolecules 42:3326–3332
46. Nagaki A, Takabayashi N, Tomida Y, Yoshida J-I (2009) Synthesis of unsymmetrically substituted biaryls via sequential lithiation of dibromobiaryls using integrated microflow systems. Beilstein J Org Chem 5. doi:10.3762/bjoc.5.16